

Optimizing the Synthesis of Folic Acid Conjugated Silver Nanoparticles by Box-Behnken Design to Target Breast Cancer Cells

Safa Furkan Soylu^{1#} , Ahmed KA Zidan^{1#} , Nazan Gökşen Tosun² , Özlem Kaplan³ , İsa Gökçe^{4*} 

¹Tokat Gaziosmanpaşa University, Faculty of Engineering and Architecture, Department of Genetics and Bioengineering, Tokat, Turkey.

²Tokat Gaziosmanpaşa University, Tokat Vocational School of Health Services, Department of Medical Services and Techniques, Tokat, Turkey

³Alanya Alaaddin Keykubat University, Rafet Kayış Faculty of Engineering, Department of Genetics and Bioengineering, Antalya, Turkey

⁴Tokat Gaziosmanpaşa University, Faculty of Pharmacy, Department of Basic Pharmaceutical Sciences, Tokat, Turkey

#These authors contributed equally to this work

*isa.gokce@gop.edu.tr

Abstract

In this study, the synthesis of folic acid-conjugated silver nanoparticles (FA&AgNPs) was optimized. FA&AgNPs were synthesized by reduction of silver nitrate with folic acid, which is widely used to target folate receptors in cancer cells. Five independent variables (stirring speed, AgNO₃ concentration, folic acid concentration, AgNO₃ volume/folic acid volume, and temperature) that were effective on silver nanoparticle synthesis were determined. Based on the independent variables, an experimental plan consisting of 46 experiments was created using the Box-Behnken design (BBD). Nanoparticle formation, physical color change, UV-Vis absorption spectroscopy, Dynamic Light Scattering (DLS) analysis, and Fourier Transform Infrared (FTIR) analysis were evaluated. The mean particle size and zeta potential of FA&AgNPs produced under optimized conditions were measured as 207±4.3 nm and -51.6 mV±2.5, respectively. Cytotoxicity tests were performed to evaluate the anticancer activity of FA&AgNPs in breast cancer cell lines. The IC₅₀ values for MDA-MB-231 breast cancer cells at 24 hours and 48 hours were 20.0 µg/mL and 16.9 µg/mL, respectively, and 26.3 µg/mL and 31.5 µg/mL for MCF-7 cells. The findings indicated that FA&AgNPs have the potential to be an effective anticancer agent in breast cancer cells.

Keywords: Folic acid, Silver nanoparticles, Breast cancer, Cell targeting, Optimization

Meme Kanseri Hücrelerini Hedeflemek için Box-Behnken Tasarımıyla Folik Asit Konjuge Gümüş Nanopartiküllerin Sentezinin Optimizasyonu

Özet

Bu çalışmada, folik asit konjuge gümüş nanopartiküllerin (FA&AgNP'ler) sentezi optimize edilmiştir. FA&AgNP'ler, kanser hücrelerinde folat reseptörlerini hedeflemek için yaygın olarak kullanılan folik asit ile gümüş nitratin indirgenmesiyle sentezlenmiştir. Gümüş nanopartikül sentezi üzerinde etkili olan beş bağımsız değişken (karıştırma hızı, AgNO₃ konsantrasyonu, folik asit konsantrasyonu, AgNO₃ hacmi/folik asit hacmi ve sıcaklık) belirlenmiştir. Bağımsız değişkenlere dayanarak, Box-Behnken tasarımı (BBD)

kullanılarak 46 deneyden oluşan bir deney planı oluşturulmuştur. Nanopartikül oluşumu, fiziksel renk değişimi, UV-Vis absorpsiyon spektroskopisi, Dinamik Işık Saçılma (DLS) analizi ve Fourier Dönüşümü Kızılötesi (FTIR) analizi ile değerlendirilmiştir. Optimize edilmiş koşullarda üretilen FA&AgNP'lerin ortalama partikül boyutu ve zeta potansiyeli sırasıyla 207 ± 4.3 nm ve -51.6 ± 2.5 mV olarak ölçülmüştür. Meme kanseri hücre hatlarında FA&AgNP'lerin antikanser etkinliğini değerlendirmek için sitotoksikite testleri yapılmıştır. 24 saat ve 48 saatte MDA-MB-231 meme kanseri hücreleri için IC_{50} değerleri 20.0 $\mu\text{g/mL}$ ve 16.9 $\mu\text{g/mL}$, MCF-7 hücreleri için ise sırasıyla 26.3 $\mu\text{g/mL}$ ve 31.5 $\mu\text{g/mL}$ olarak bulunmuştur. Bulgular, FA&AgNP'lerin meme kanseri hücrelerinde etkili bir antikanser ajan olma potansiyeline sahip olduğunu göstermiştir.

Anahtar Kelimeler: Folik asit, Gümüş nanopartiküller, Meme kanseri, Hücre hedefleme, Optimizasyon

1. INTRODUCTION

Cancer is an important public health issue that ranks second among worldwide causes of mortality [1]. Developing novel nanoscale chemotherapy agents is increasingly significant in addressing the adverse effects of conventional chemotherapy approaches [2]. Nanoparticles have become highly attractive due to their numerous advantages, such as drug delivery and targeting capabilities [3]. Metallic nanoparticles, nanostructured materials composed of pure metals or their compounds, offer a novel platform for targeted drug delivery, enabling the treatment of diverse diseases within a specific and controlled environment [4]. As one of the metallic nanoparticles with chemical stability, silver nanoparticles (AgNPs) have distinctive features such as strong electrical conductivity, catalytic activity, and antibacterial activities [5,6]. There has been a surge of research investigating the utilization of AgNPs in anticancer therapy in recent years [7-9]. AgNPs can interact with cells and cause cell membrane disruption, affect electron transport chains, generate radicals, interfere with protein synthesis by interacting with ribosomes, affect enzyme function by interacting with enzymes, and cause DNA damage by interacting with DNA [10].

Folic acid (FA), a recognized ligand for folate receptors, has been used to develop nanoformulations with surface functionalization for specific targeting of breast cancer cells [11]. FA plays an important role in the biosynthesis of pyrimidines and purines, which are necessary for DNA synthesis, methylation, and repair. FA is a cofactor in synthesizing purines and pyrimidines in amino acids and DNA/RNA structures [12]. Most cancer tissues overexpress folate receptors, including lung, ovarian, colorectal, brain, breast, epithelial, renal, and cervical malignancies. This expression can target chemicals and medicinal substances directly to malignant cells [13]. Targeting folate receptors is appealing due to their restricted overexpression in healthy tissues and organs. The harmful effects of chemotherapeutic medicines can be decreased by employing folate as a targeting ligand for chemotherapy because folate will preferentially bind to cancer cells overexpressing folate receptors while binding to normal cells at a lower amount [14]. The use of folic acid-conjugated nanocarriers is a preferred method to achieve selective delivery of chemotherapeutic drugs in malignancies that overexpress folate receptors. In this way, many folic acid-conjugated nanoparticles based on polymeric [15], lipid [16], dendrimer [17] and metallic [18] carriers have been designed.

This study focused on optimizing FA&AgNPs synthesis using the Box-Behnken design (BBD). Response surface analysis was used to evaluate the independent variable-response relationship based on particle size and size distribution analysis, and optimal synthesis conditions were determined. UV-Vis spectrophotometry, Dynamic Light Scattering (DLS), and Fourier Transform Infrared (FTIR) analyses were used to characterize the FA&AgNPs. In addition, the effect of FA&AgNPs synthesized under optimal conditions on cell viability in breast cancer cell lines (MDA-MB-231 and MCF-7) was analyzed using the MTT assay. MCF-7 and MDA-MB-231 cell lines are well-known and widely used models representing breast cancer [19]. The expression levels of folate receptors in these two cell lines are different. MDA-MB-231 cells express higher levels of folate receptors than MCF-7 cells [20]. In this respect, these two cell lines were chosen to examine the comparative cytotoxic effects of the FA&AgNPs.

2. MATERIAL AND METHOD

2.1 Material

Silver nitrate (AgNO_3) was obtained from Carlo Erba, 3-(4,5-dimethylthiazol-2-yl)-2,5-diphenyltetrazolium bromide (MTT) and Folic acid ($\text{C}_9\text{H}_{19}\text{N}_7\text{O}_6$) were purchased from Serva. Dulbecco's Modified Eagle Medium (DMEM) High Glucose, fetal bovine serum (FBS, heat-inactivated), penicillin-streptomycin solution, L-glutamine, phosphate-buffered saline (PBS), and trypsin-EDTA were obtained from Biological Industries. The American Type Culture Collection (ATCC) provided the MDA-MB-231 and MCF-7 cell lines.

2.2 Method

2.2.1 Optimization of synthesis of FA&AgNPs using Box-Behnken design

The synthesis of FA&AgNP was accomplished through a green synthesis approach, eliminating the need for harsh chemicals. It involved mixing a solution of AgNO_3 with a solution of FA in specific proportions and at a certain temperature, resulting in the reduction of Ag^+ ions by FA molecules. A graphical summary of the study, including the physical and chemical characterization of FA&AgNP, is depicted in Figure 1.

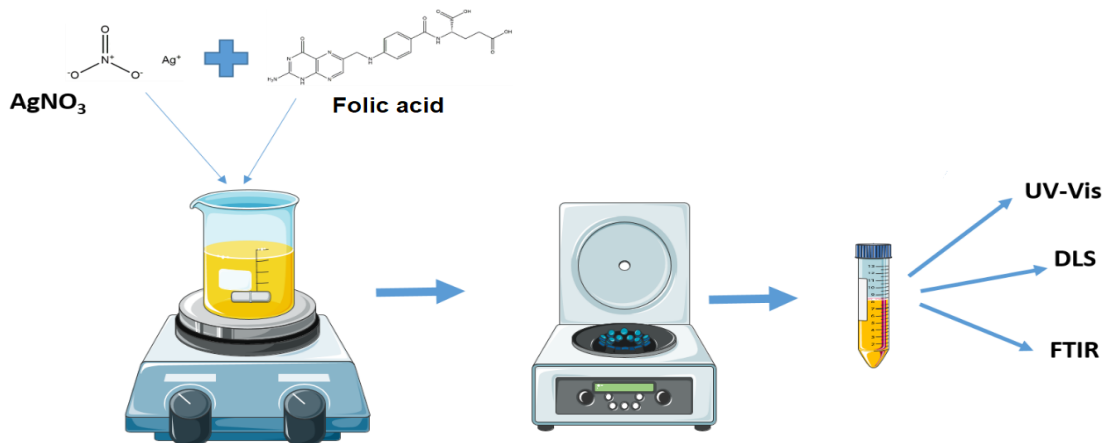


Figure 1. Synthesis and characterization of FA&AgNPs

Five independent variables that could affect the green synthesis of FA&AgNPs were determined. These independent variables are as follows: stirring speed, AgNO_3 concentration, FA concentration, $V(\text{AgNO}_3)/V(\text{FA})$ volumetric ratio, and temperature. The ranges in which the independent variables were determined (Table 1). FA&AgNPs were optimized by Box-Behnken design using Design Expert® 11.0 software.

Table 1. Independent variables

Factor	Name	Unit	Min	Max	Mid.
A	Stirring Speed	rpm	250	1000	625
B	AgNO_3 concentration	mM	1	5	3
C	Folic acid concentration	mM	1	5	3
D	AgNO_3 volume/folic acid volume	-	0,1	0,5	0,3
E	Heat	°C	25	60	42,5

2.2.2 Synthesis of FA&AgNPs

To perform the synthesis of FA&AgNPs, 1 and 10 mM AgNO₃ stock solution and 20 mM FA stock solution were prepared. AgNO₃ and FA concentrations required for each experiment were diluted from stock solutions. AgNO₃ with the concentrations given in Table 2 was taken into beakers with a volume of 10 mL. AgNO₃ solution was taken on a magnetic stirrer, and the temperature and stirring speeds were adjusted according to the values given in Table 2. Then, FA solutions were added dropwise into AgNO₃ solutions and waited for one hour to complete the reaction. DLS analysis was performed for each of the synthesized FA&AgNPs, and the most suitable one was determined according to size, size distribution, and zeta potential. FA&AgNPs were centrifuged for 15 minutes at 13000 rpm. Free silver and FA molecules in the supernatant were eliminated, and FA&AgNPs in the pellet were washed twice with distilled water before being used in the next steps.

2.2.3 Characterization of FA&AgNPs

2.2.3.1 UV-Vis analysis

For proving the synthesis of FA&AgNPs, a UV-Vis spectrophotometer (DeNoVIX) was used to measure the wavelength range of 200-800 nm. Ultra-purified de-ionized water was used as a blank.

2.2.3.2 FTIR analysis

FTIR shows the presence of various functional groups (such as proteins, amino acids, and aldehydes) around the synthesized FA&AgNPs. FA&AgNPs were scanned in the range of 400-4000 cm⁻¹ using the Jasco FT/IR 4700 instrument to obtain a good signal-to-noise ratio.

2.2.3.3 DLS analysis

DLS (HORIBA-SZ-100) was used to assess the size, polydispersity, and zeta potential of FA&AgNPs. The measurements were carried out by loading FA&AgNP samples into the electrode cells and under computer control. The cell was washed with deionized water before each measurement.

2.2.4 Biological activity determination of FA&AgNPs

2.2.4.1 Cell culture

The cytotoxic effects of FA&AgNPs on MDA-MB-231 and MCF-7 breast cancer cell lines were investigated. First, MCF-7 and MDA-MB-231 cell lines were cultured in T75 flasks in DMEM High Glucose medium containing 10% FBS, 1% L-glutamine, and 0.1% gentamicin. Cells seeded in T75 flasks were incubated in a 37 °C incubator with 5% CO₂ until they reached 90% confluency.

2.2.4.2 Cell viability analysis

For cell viability analysis, cells were first seeded into 96-well plates at a concentration of 5 x 10⁴ cells/mL in each well. Then, these plates were incubated for 24 hours in an incubator at 37 °C containing 5% CO₂. Following the incubation, these cells were treated with FA&AgNPs in the concentration range of 100 µg/mL-1.56 µg/mL and left to incubation (at 37 °C containing 5% CO₂) for 24 and 48 hours. Since viable cells form formazan salts using MTT, the number of viable cells in each well was determined by adding MTT dye to each well. The absorbance value of each well in the plates at a wavelength of 570 nm was measured using a Microplate Reader Spectrophotometer. Cell viability was calculated with the GraphPad 8.1 program. Statistical analysis and comparable data sets were analyzed using GraphPad Prism 8.0 software and a two-way ANOVA with the Sidak test. Statistical significance was determined as a probability value of 0.05.

3. RESULTS AND DISCUSSION

3.1 Optimization of FA&AgNP Synthesis with Box-Behnken Design

The experimental results yielded the size and distribution outputs presented in Table 2.

Table 2. Size and size distributions of FA&AgNPs

Std	Stirring speed(rp m)	AgNO ₃ cons. (mM)	FA cons. (mM)	V(AgNO ₃)/V(FA)	Heat (°C)	Particle size (nm)	PDI
1	250	1	3	0.3	42.5	778	0.664
2	1000	1	3	0.3	42.5	1151.2	0.592
3	250	5	3	0.3	42.5	443.7	1.198
4	1000	5	3	0.3	42.5	234.4	0
5	625	3	1	0.1	42.5	417.5	1.834
6	625	3	5	0.1	42.5	294.8	0
7	625	3	1	0.5	42.5	371.2	2.359
8	625	3	5	0.5	42.5	295.2	1.688
9	625	1	3	0.3	25	784.5	0.662
10	625	5	3	0.3	25	175.3	0
11	625	1	3	0.3	60	940.3	0.655
12	625	5	3	0.3	60	0	0
13	250	3	1	0.3	42.5	406.1	1.987
14	1000	3	1	0.3	42.5	190.9	4.28
15	250	3	5	0.3	42.5	1894.7	1.421
16	1000	3	5	0.3	42.5	250.5	2.863
17	625	3	3	0.1	25	372.5	2.326
18	625	3	3	0.5	25	316.8	0
19	625	3	3	0.1	60	378.5	1.82
20	625	3	3	0.5	60	128.8	0
21	625	1	1	0.3	42.5	590.1	1.371
22	625	5	1	0.3	42.5	9366.4	5.844
23	625	1	5	0.3	42.5	615	0.655
24	625	5	5	0.3	42.5	9154.6	0.444
25	250	3	3	0.1	42.5	297.4	2.657
26	1000	3	3	0.1	42.5	238.5	3.181
27	250	3	3	0.5	42.5	1345.2	0
28	1000	3	3	0.5	42.5	333.2	1.659
29	625	3	1	0.3	25	345.5	2.626
30	625	3	5	0.3	25	349.9	2.102
31	625	3	1	0.3	60	1199.1	0
32	625	3	5	0.3	60	4320.6	1.595
33	250	3	3	0.3	25	961.1	0.722
34	1000	3	3	0.3	25	208.5	2.578
35	250	3	3	0.3	60	1213.2	0.681
36	1000	3	3	0.3	60	372.2	3.041
37	625	1	3	0.1	42.5	539.8	0.96
38	625	5	3	0.1	42.5	0	0
39	625	1	3	0.5	42.5	668.2	0.638
40	625	5	3	0.5	42.5	2559	1.139
41	625	3	3	0.3	42.5	181.8	2.8
42	625	3	3	0.3	42.5	230.5	3.222

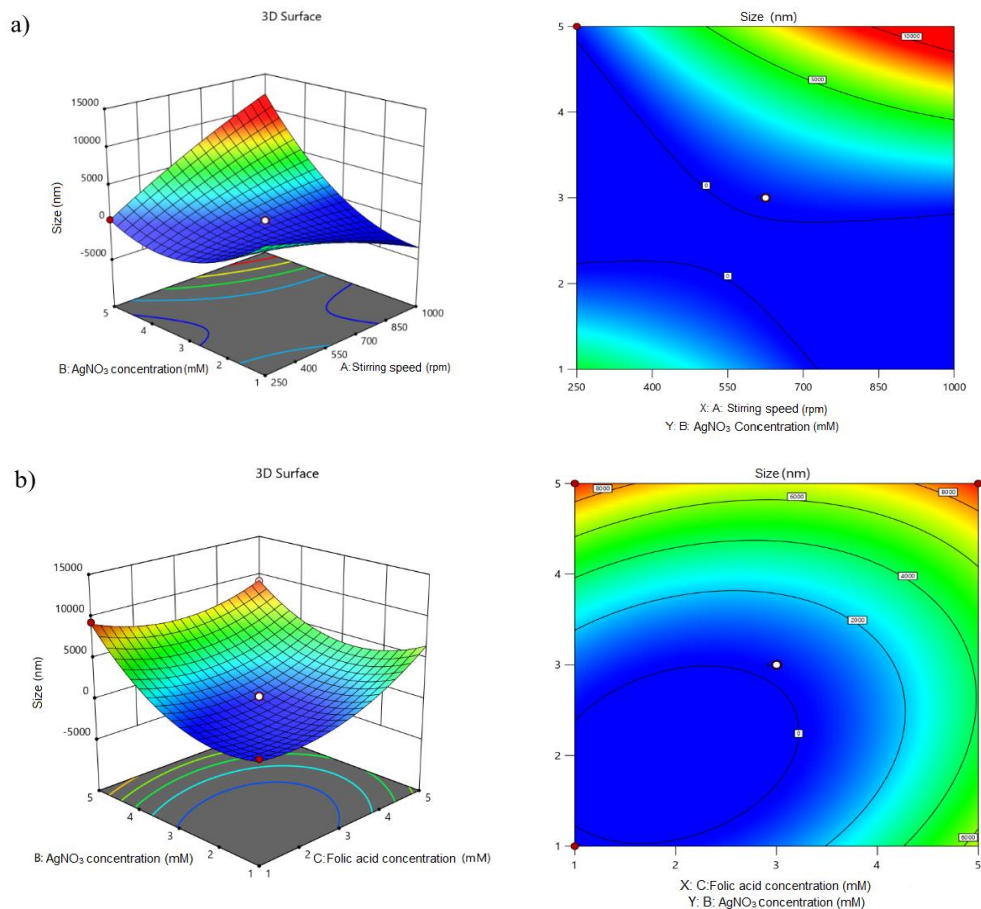
43	625	3	3	0.3	42.5	400.7	1.861
44	625	3	3	0.3	42.5	428.2	0
45	625	3	3	0.3	42.5	363.5	1.326
46	625	3	3	0.3	42.5	89.1	0

3.1.1 Optimization results based on particle size output

Size and size distribution data were entered as output for BBD analysis. Outputs depending on particle size were obtained. The polynomial equation for the response factor was created. The correlation coefficient (R^2) was calculated as 0.9943 based on the obtained data.

$$\begin{aligned} \text{Particle Size} = & 294.125 + 997.54293379686 * A + 2893.2610338573 * B + 1584.5853083434 * C - \\ & 1923.1442563482 * D + 1776.186766928 * E + 4865.6142911125 * AB + 970.80808645707 * AC + \\ & 1970.4942563482 * AD - 2655.2392004232 * AE - 1541.1424652358 * BC - 1994.1145329504 * BD + \\ & 3197.8610338573 * BE - 1786.3225665054 * CD + 121.08188482467 * CE + 1773.1867669287 * DE - \\ & 590.56795646916 * A^2 + 3710.0391475212 * B^2 + 2306.2389737001 * C^2 - 407.62583887545 * D^2 - \\ & 1647.9462439541 * E^2 \end{aligned}$$

Graphics showing how the size changes according to the independent variables are given in Figure 2.



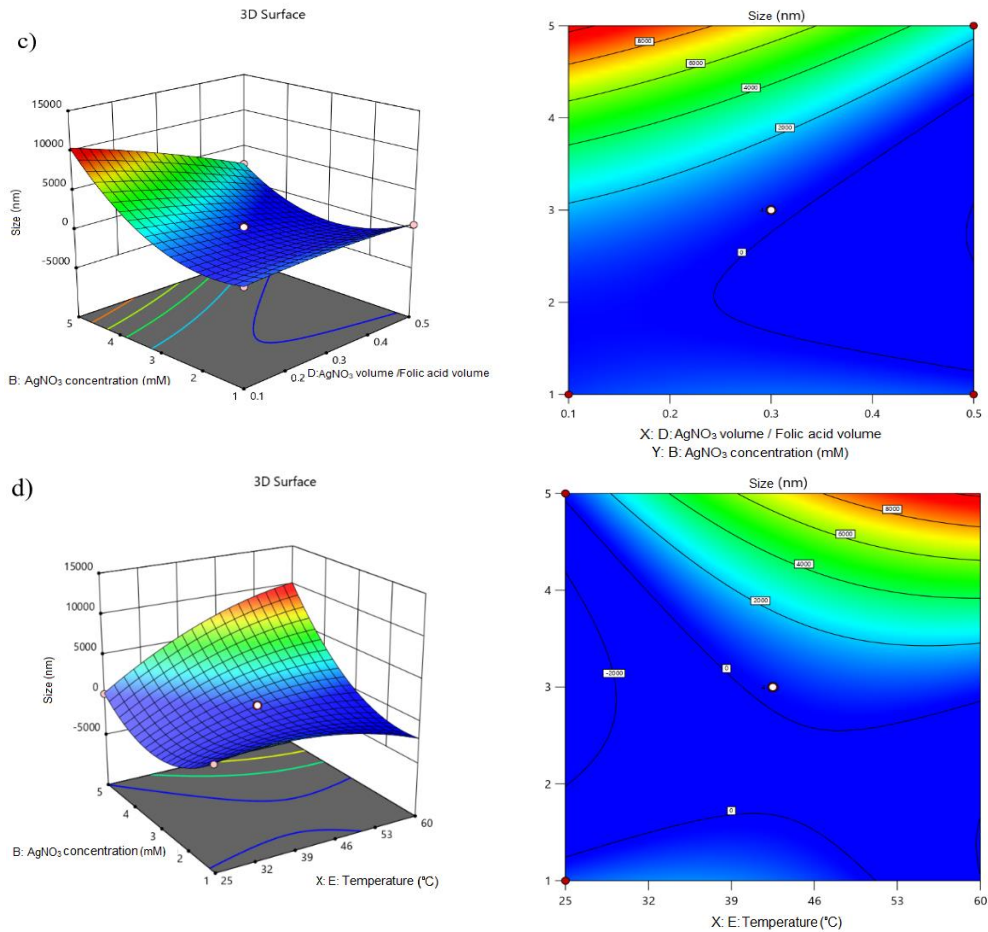


Figure 2. Projection and 3D response surface plots of the parameters affecting the particle size of synthesized FA&AgNPs. (a) AgNO₃ concentration and Stirring speed. (b) AgNO₃ and FA concentration. (c) AgNO₃ concentration and V(AgNO₃)/V(FA). (d) AgNO₃ concentration and temperature.

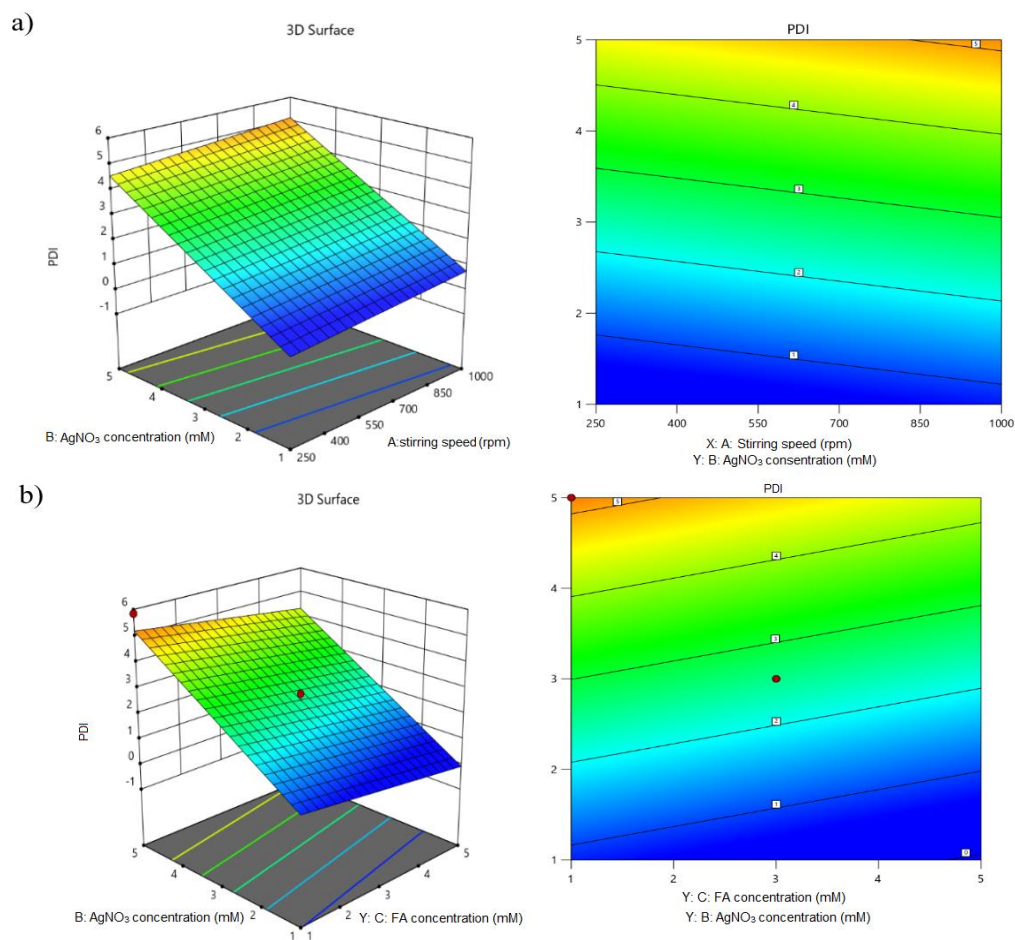
According to the graphs given in Figure 2, a) It was observed that increasing both the stirring speed and AgNO₃ concentration simultaneously increased particle sizes. Similarly, when the stirring speed and AgNO₃ concentration were reduced simultaneously, a decrease in particle sizes was observed. b) The size of the particles was found to increase with higher concentrations of AgNO₃ and folic acid (FA). Conversely, when AgNO₃ and FA concentrations were kept low, nanoparticles with nano-scale sizes could be achieved. c) It was found that an increase in the V(AgNO₃)/V(FA) ratio led to larger particle sizes. Particularly, particle sizes close to the desired target were obtained when the AgNO₃ concentration was below 3 mM, and the V(AgNO₃)/V(FA) ratio approached its upper values. d) Box-Behnken design (BBD) results showed that the AgNO₃ concentration should be kept at the lowest levels while increasing the temperature to obtain nano-sized particles. Theoretical considerations suggested particle sizes would be at the desired levels when the temperature and AgNO₃ concentration were low. In summary, these findings demonstrate that the particle size of FA&AgNPs can be influenced by the Stirring speed, AgNO₃ concentration, V(AgNO₃)/V(FA) ratio, and temperature. By optimizing these variables, it is possible to control the particle sizes, especially by employing lower AgNO₃ concentrations and temperatures.

3.1.2 Optimization results based on output-to-size distribution (PDI)

A polynomial equation was formulated to represent the response factor. After analyzing the data, the correlation coefficient (R^2) was calculated as 0.9148.

$$\text{PDI} = 2.56055252263 + 0.29602641919865 * A + 2.1877807522279 * B - 0.44682453862887 * C - 0.50984250228054 * D + 0.22764286716722 * E$$

Figure 3 presented graphical representations illustrating the size variations corresponding to the independent variables. Additionally, in Figure 3, the PDI values showed an increasing trend from blue to red. During the evaluation of the PDI results, it can be concluded that the size distribution within the range of 0-0.7 is predominantly monodisperse. Hence, PDI values falling within this range were deemed the most favorable for nanoparticle synthesis. On the other hand, PDI values outside this range were characterized as polydisperse, indicating a broader size distribution.



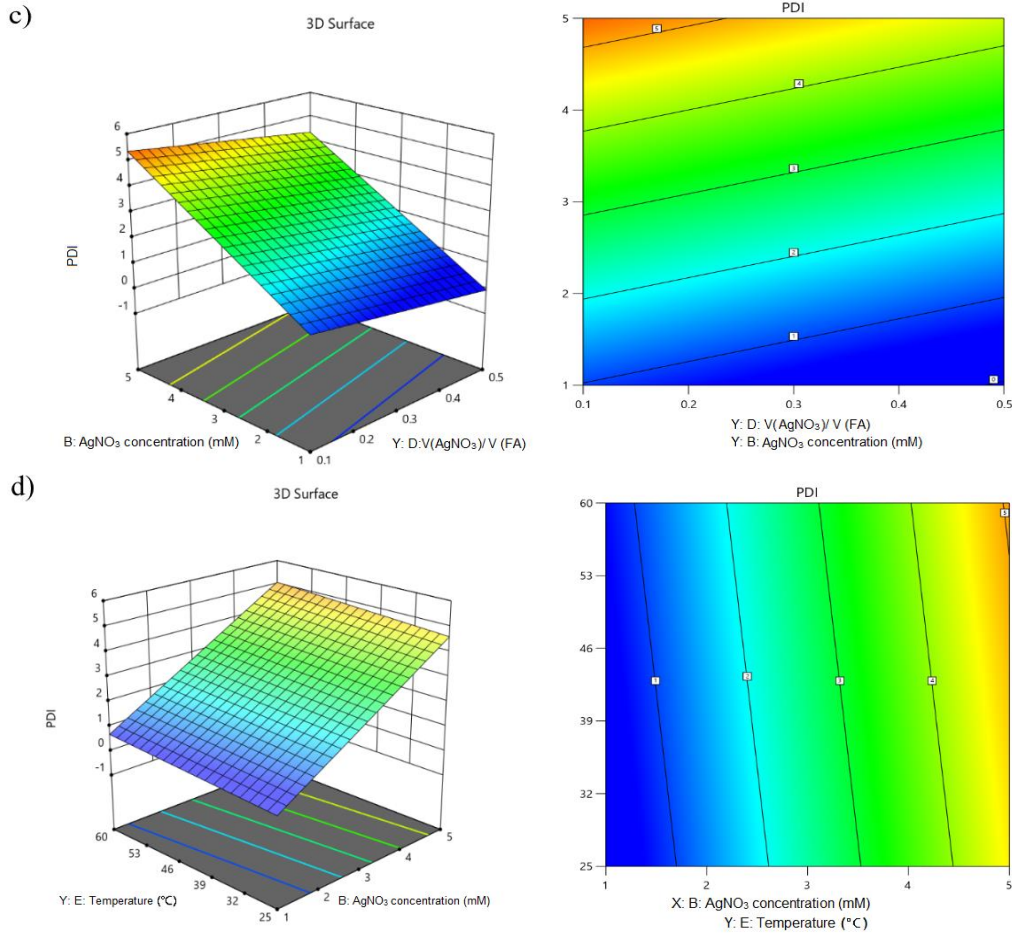


Figure 3. Projection and 3D response surface plots of the parameters affecting the PDI values of synthesized FA&AgNPs. (a) AgNO₃ concentration and Stirring speed. (b) AgNO₃ and FA concentration. (c) AgNO₃ concentration and V(AgNO₃) / V(FA) (d) AgNO₃ concentration and temperature.

Based on the observations made in Figure 3, a) Simultaneously increasing the stirring speed and AgNO₃ concentration resulted in an undesired size distribution in the particles. However, by maintaining a flexible Stirring speed range of 250-1000 rpm and employing low AgNO₃ concentrations (1-2 mM), the PDI value can be maintained at desired levels. b) The PDI value tended to increase with higher FA concentrations and lower AgNO₃ concentrations. It was determined that the PDI value might be kept within the required range by reducing the FA concentration to 1 mM and keeping the AgNO₃ values between 1-2 mM. c) Increasing both the V(AgNO₃)/V(FA) ratio and the AgNO₃ concentration raised the PDI value. However, the appropriate PDI values were obtained by maintaining a low V(AgNO₃)/V(FA) ratio and keeping AgNO₃ concentrations within the range of 1-2 mM. d) The Box-Behnken design (BBD) findings showed that raising the temperature while retaining low AgNO₃ concentrations can achieve the appropriate PDI values. In summary, the data revealed that regulating the Stirring speed, AgNO₃ concentration, V(AgNO₃)/V(FA) ratio and temperature were the best conditions for reaching desirable PDI values. It is feasible to generate nanoparticles with the required size distribution by carefully modifying these factors.

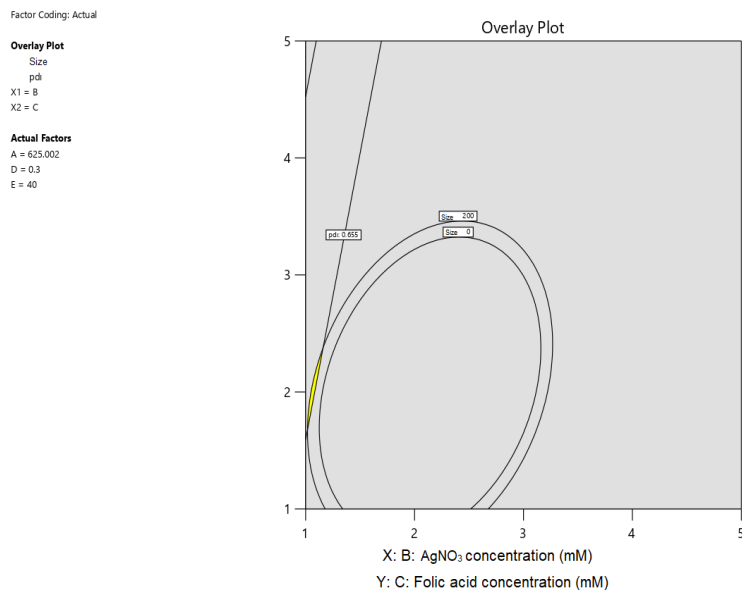


Figure 4. Graph showing the optimized region in yellow and the marked point as selected FA & AgNPs

The optimization of FA&AgNPs using the BBD was carried out as previously reported [21,22]. The desirability function neared a value of one, indicating that the goal response variable was successfully achieved. The optimal conditions for FA&AgNP synthesis were determined based on the yellow region depicted in Figure 4. This region was determined by setting target values for specific independent variables while considering relevant laboratory conditions. The target values for the optimization were as follows: AgNO₃ concentration of 1 mM, V(AgNO₃)/V(FA) ratio of 0.3, temperature of 40°C, stirring speed of 625 rpm, and FA concentration of 2.4 mM.

3.2 Characterization of FA&AgNPs

UV-Vis spectrophotometry was used to characterize the FA&AgNPs synthesized under optimal conditions, and the results were presented in Figure 5. The spectrum of FA&AgNPs exhibited a peak at 419 nm. Additionally, the maximum absorbance wavelength for FA was determined to be 300 nm. Notably, the presence of a peak in the 300-500 nm range for FA&AgNPs, distinct from the peak of FA, serves as evidence for the successful synthesis of FA&AgNPs. As stated in previous studies, the absorption peak in the 300-500 nm region was observed when silver nitrate was reduced to silver nanoparticles. [23,24]. In this study, FA was employed as a reduction agent for silver ions. The prominent bright yellow coloration further confirms the formation of AgNPs. Chowdhuri et al. have demonstrated that FA is an effective reduction agent, providing stability to AgNPs and preventing their aggregation. Consequently, AgNPs synthesized using this approach have exhibited enhanced stability for a period exceeding one year [25].

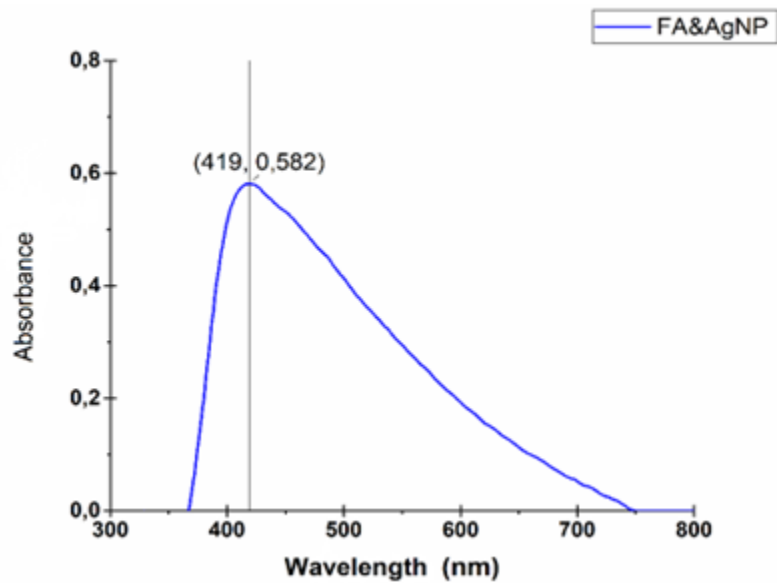


Figure 5. UV-Visible spectra of FA&AgNPs

FTIR analysis was performed to characterize the chemical reduction of silver ions by FA. FTIR analysis results of FA were compared with FTIR analysis results of FA&AgNPs (Figure 6).

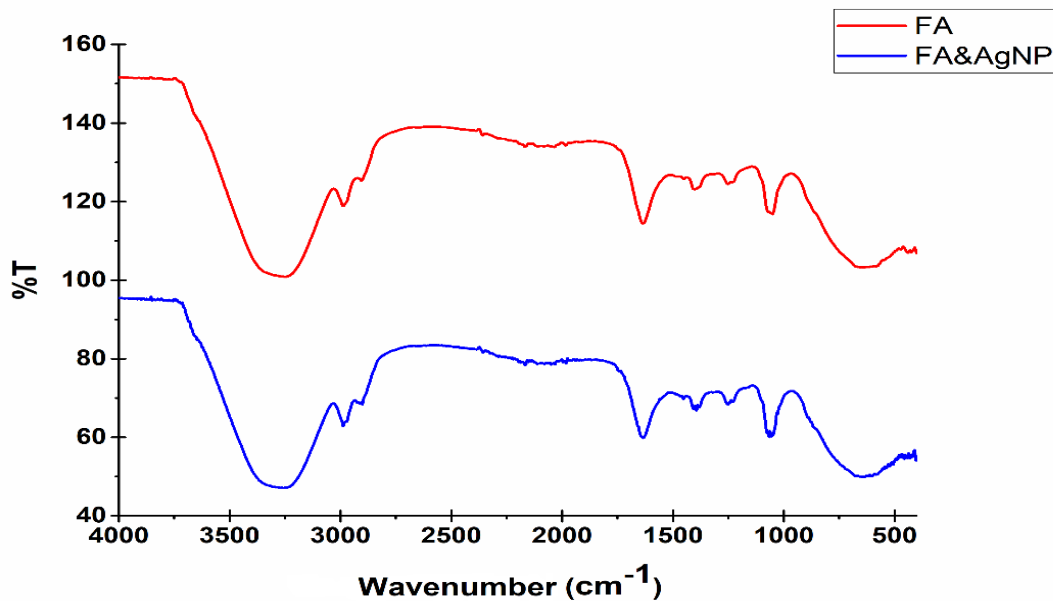


Figure 6. FTIR analysis of FA&AgNPs

Peaks expressing specific information regarding folic acid conjugation were analyzed. In the free folic acid spectra, the distinctive IR absorption peaks at 1633 cm⁻¹ and 1487 cm⁻¹ were found due to the N-H bending vibration of the CONH group and the absorption band of the phenyl ring, respectively [25]. A prominent peak around 3293 cm⁻¹ was characterized as an O-H stretching vibration. The same peaks may be detected in FA&AgNPs, proving chemically that FA binds to Ag⁺ ions.

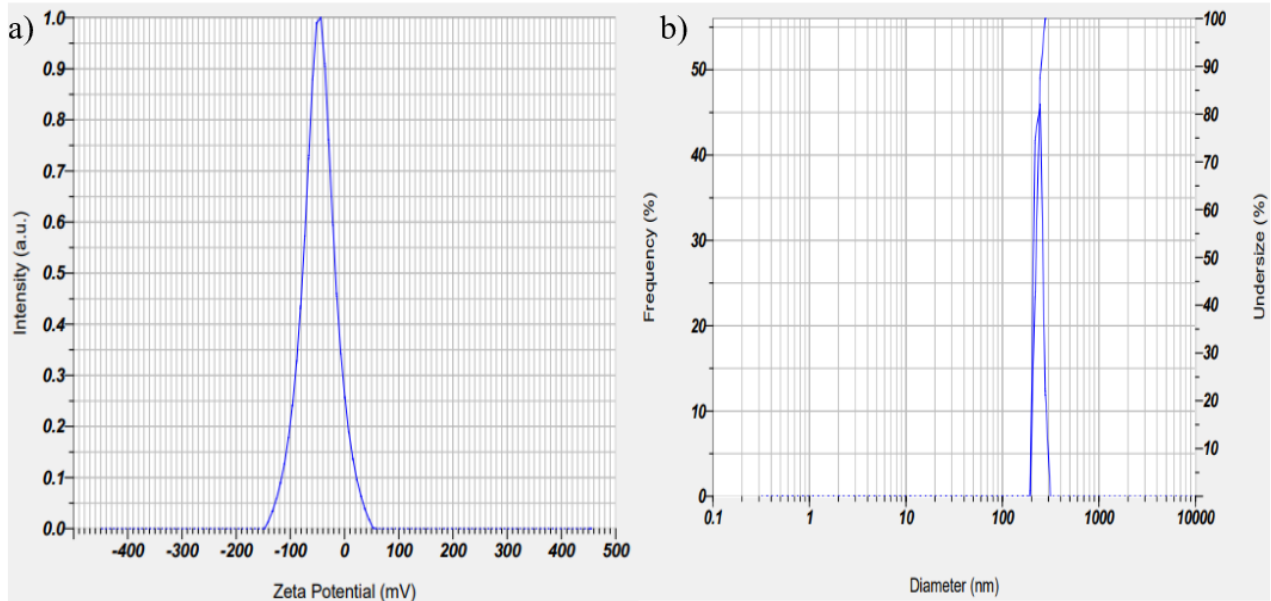


Figure 7. a) DLS of FA&AgNPs, b) Zeta potential of FA&AgNPs

The size of FA&AgNP was determined using DLS, as shown in Figure 7. The FA&AgNPs had an average size of 207 ± 4.3 nm. The polydispersity index (PDI) values are indicative of the uniformity of nanoparticle distribution, and a PDI value exceeding 0.7 suggests a non-uniform distribution of nanoparticles [26]. The nanoparticles were distributed uniformly (polydispersity index: 0.655). In addition, the zeta potential value of the FA&AgNPs was found to be -51.6 ± 2.5 mV. A zeta potential value ranging from -30 mV to +30 mV signifies the excellent dispersion and long-term stability of nanoparticles, reducing the likelihood of aggregation [26]. The presence of a negative charge on the surface of the nanoparticles implied that they are highly stable.

3.3 Cytotoxic Effect of FA AgNPs on Breast Cancer Cell Lines

MTT analysis was used to assess the cytotoxic effects of FA&AgNP on MDA-MB-231 and MCF-7 cell lines. Graphs of concentration-dependent cell viability determined by MTT analysis are shown in Figure 8.

Figure 8 was plotted by calculating the data obtained after 24 and 48 hours for both cell lines with the GraphPad 8.1 program.

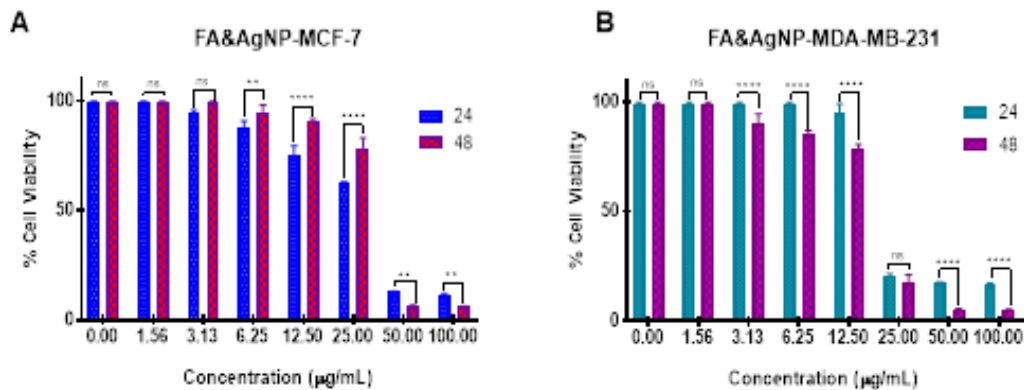


Figure 8. Cytotoxic effect of FA&AgNPs on MCF-7 (A) and MDA-MB-231 (B). The results are shown as the mean SEM (n = 3). *p < 0.05, **p < 0.01, ***p < 0.001 and ****p < 0.0001 represent statistical significance

The concentration value at which cell viability is reduced by 50% corresponds to the concentration value at which 50% of the cells are inhibited. This value is called IC_{50} in this study; it was calculated using GraphPad 8.1 software and presented in Table 3.

Table 3. IC_{50} values of FA&AgNPs after 24 h and 48 h on MDA-MB-231 and MCF-7 cell lines

Cell lines	MCF-7		MDA-MB-231	
Time	24 h	48 h	24 h	48 h
IC_{50} ($\mu\text{g/mL}$)	26.30 ± 0.003	31.50 ± 0.002	20.00 ± 0.004	16.99 ± 0.003

Two distinct cell lines derived from breast cancer were selected to assess the cytotoxic potential of folic acid-functionalized AgNPs. The MDA-MB-231 and MCF-7 cell lines exhibit contrasting responses to hormone therapies. MCF-7 cells possess both estrogen receptor (ER) and progesterone receptor (PR) while lacking human epidermal growth factor receptor 2 (HER2) [27]. Conversely, MDA-MB-231 represents a triple-negative breast cancer (TNBC) cell line devoid of all three receptors (ER, PR, and HER2), rendering hormone therapy ineffective. MDA-MB-231 and MCF-7 cells express folate receptors, although MDA-MB-231 cells express higher levels of FR- α than MCF-7 cells [20]. In this study, FA&AgNPs showed relatively more cytotoxic activity against MDA-MB-231 cells than MCF-7 cells. This result was attributed to MDA-MB-231 cells expressing higher levels of folate receptors.

Folate receptor-targeting nanoparticles have been studied to treat different cancer therapies, including breast cancer. El-Hammadi et al. developed PLGA nanoparticles with PEG coating and folic acid decoration. These 5-FU loaded-nanoparticles showed superior cytotoxic effects over non-targeting PLGA-based NPs in both HT-29 colon cell lines and MCF-7 breast cancer cell lines [28]. In another study, Erdogar et al. designed folate-conjugated β -cyclodextrins loaded with paclitaxel. Conjugation of paclitaxel with folate-conjugated cyclodextrin showed that it increased the sensitivity and cellular uptake efficiency of breast cancer cells towards the developed NPs, thus reducing the side effects of paclitaxel[29].

Karuppaiah et al. synthesized folic acid-conjugated silver nanoparticles and investigated their combined effect with gemcitabine (GEM) on breast cancer cells. It has been demonstrated that FA serves as a potent reducing and coating agent for cancer cells with folate receptors. FA-coated GEM-AgNPs exhibited synergistic effects and increased selectivity against MDA-MB-453 cells. FA-coated GEM-AgNPs demonstrated increased cytotoxicity ($IC_{50}=35.34 \mu\text{M}$) compared to the individual use of GEM and AgNPs, resulting in reduced dose-dependent toxicity. Furthermore, the induction of apoptotic cell death by FA-GEM-AgNPs in the MDA-MB-453 cell line was observed [30]. Banu et al. synthesized folic acid conjugated polymer-gold composite nanoparticles (GNPs) that combined doxorubicin (DOX) with laser photothermal treatment. The surface of GNPs was changed with folate, and polyethylene glycol (PEG) was designed to carry DOX to the targeted breast cancer cells. The folic acid-conjugated DOX-loaded polymeric GNPs and laser photothermal treatment outperformed DOX alone, notably against breast cancer cells with high folate expression (MDA-MB-231) [31,32]. DOX conjugated with N-acetyl glucosamine or folate-functionalized mesoporous silica nanoparticles (DOX-NAG-MSNPs or DOX-FA-MSNPs) has been synthesized by Pramod et al. DOX-NAG-MSNPs had stronger cellular absorption and cytotoxicity than DOX-FA-MSNPs, particularly in MDA-MB-231 and MCF-7 cells. DOX-FA-MSNPs and DOX-NAG-MSNPs demonstrated better DOX transport to specific breast cells as compared to free DOX [33,34]. Considering the previous studies and the data obtained in our study, using folic acid-conjugated nanoparticles for targeting the folate receptor is considered a promising approach to treating breast cancer. It has been reported that folic acid-conjugated nanocarrier systems can bind selectively to the folate receptor

on the surface of cancer cells and be carried into the cell via clathrin-mediated endocytosis [35,36]. Circulating folic acid-conjugated transporters bind to folate receptors on the surface of cancer cells, resulting in invagination, internalization, and vesicle formation. When the pH within the vesicle decreases, the folic acid-conjugated chemotherapeutic drug is released into the cytosol, causing the desired pharmacological action in cancer cells. This impact either stops cell division or causes apoptosis [37]. As a result, the FA&AgNPs synthesized in this study may be delivered to the cells via clathrin-mediated endocytosis by binding to the folate receptor in breast cancer cells. It has been shown in numerous studies that silver nanoparticles exhibit cytotoxic effects on cancer cells through mechanisms such as disrupting cell membranes, interfering with electron transport chains, creating radicals, disrupting protein synthesis through ribosome interaction, affecting enzymes, and triggering DNA damage [7,10]. Therefore, FA&AgNPs that can specifically bind to the folate receptor may have a cytotoxic effect on cells through these mechanisms.

In recent years, investigations have been carried out to investigate the green synthesis of silver nanoparticles using plant extracts and their anticancer effects on breast cancer. Santhoshkumar et al. synthesized silver nanoparticles from the liquid extract obtained from *Gymnema sylvestris* leaves by green synthesis and determined the IC_{50} value as $44 \pm 0.8 \mu\text{g/mL}$ on MDA-MB-231 cells after 24h. Darvish et al. silver nanoparticles were synthesized using *Ducrosia Anethifolia* aqueous extract and investigated the cytotoxic effect of these nanoparticles on MDA-MB-231 and MCF-7 cells. After 24 h, IC_{50} values were calculated as $45.24 \pm 2.96 \mu\text{g/mL}$ and $33.78 \pm 3.54 \mu\text{g/mL}$, respectively [38]. The metabolite content of the extract used in the synthesis of FA&AgNPs and the size, zeta potential, and particle size distribution of FA&AgNPs are the factors affecting the toxicity of the FA&AgNPs produced in this study on breast cancer cells. The IC_{50} values of the FA&AgNPs obtained in this study on MDA-MB-231 and MCF-7 cells after 24 h were calculated as $20.0 \mu\text{g/mL}$ and $26.3 \mu\text{g/mL}$, respectively. After 48 hours, IC_{50} values on MDA-MB-231 and MCF-7 cells were found to be $16.99 \mu\text{g/mL}$ and $31.50 \mu\text{g/mL}$, respectively. While FA&AgNPs showed a dose- and time-dependent cytotoxic effect on the MDA-MB-231 cell line, the time-dependent cytotoxic effect did not increase on MCF-7 cell lines. FA&AgNPs exhibited higher cytotoxicity than MCF-7 in MDA-MB-231 cell lines, indicating that they may be more effective in this cell line. The possible reason for this effect is that MDA-MB-231 cells express higher levels of folate receptors than MCF-7 cells.

4. CONCLUSION

In this study, FA&AgNPs were synthesized using AgNO_3 salt and FA as a reducing agent. The synthesis of FA&AgNPs was systematically optimized using the Box-Behnken design. The experimental design consisted of 46 different trials generated theoretically based on five independent variables (Stirring speed, AgNO_3 concentration, FA concentration, $V(\text{AgNO}_3)/V(\text{FA})$ ratio, and temperature). Nanoparticle formation was physically detected by monitoring the color transformation and absorption band based on the surface plasmon resonance of the nanoparticles. FTIR analysis revealed the binding of FA to Ag^+ ions. The AgNO_3 concentration was found to be highly influential in nanoparticle formation efficiency. The optimal conditions were determined as a stirring speed of 625 rpm, AgNO_3 concentration of 1 mM, $V(\text{AgNO}_3)/V(\text{FA})$ ratio of 0.3, and FA concentration of 2.4 mM. The average size and zeta potential of the synthesized FA&AgNPs were measured as $207 \pm 4.3 \text{ nm}$ and $-51.6 \pm 2.5 \text{ mV}$, respectively. Cytotoxicity results on breast cancer cell lines MDA-MB-231 and MCF-7 showed that FA&AgNPs could potentially serve as agents with anticancer activity. In conclusion, the synthesized and optimized FA&AgNPs in this study hold promise as a novel agent for potential use in breast cancer treatment in future studies.

ACKNOWLEDGEMENTS

This study received support from the Turkish Scientific and Technical Research Council (TUBITAK) under grant number TUBITAK-2209A (Project number: 1919B012106589).

REFERENCES

- [1] Sung H., Ferlay J., Siegel R.L., Laversanne M., Soerjomataram I., Jemal A., Bray F. (2021). "Global Cancer Statistics 2020: GLOBOCAN Estimates of Incidence and Mortality Worldwide for 36 Cancers in 185 Countries." *CA: A Cancer Journal for Clinicians* 71, 209-249. <https://doi.org/10.3322/caac.21660>
- [2] Yao Y., Zhou Y., Liu L., Xu Y., Chen Q., Wang Y., Wu S., Deng Y., Zhang J., Shao A. (2020). "Nanoparticle-Based Drug Delivery in Cancer Therapy and Its Role in Overcoming Drug Resistance." *Front Mol Biosci* 7, 193. [10.3389/fmolb.2020.00193](https://doi.org/10.3389/fmolb.2020.00193)
- [3] Khan I., Saeed K., Khan I. (2019). "Nanoparticles: Properties, applications and toxicities." *Arabian Journal of Chemistry* 12, 908-931. <https://doi.org/10.1016/j.arabjc.2017.05.011>
- [4] Chandrakala V., Aruna V., Angajala G. (2022). "Review on metal nanoparticles as nanocarriers: current challenges and perspectives in drug delivery systems." *Emergent Materials* 5, 1593-1615. [10.1007/s42247-021-00335-x](https://doi.org/10.1007/s42247-021-00335-x)
- [5] Gökşen Tosun N., Kaplan Ö., Türkekul İ., Gökçe İ., Özgür A. (2022). "Green synthesis of silver nanoparticles using *Schizophyllum commune* and *Geopora sumneriana* extracts and evaluation of their anticancer and antimicrobial activities." *Particulate Science and Technology* 40, 801-811. [10.1080/02726351.2021.2010846](https://doi.org/10.1080/02726351.2021.2010846)
- [6] Kaplan Ö., Gökşen Tosun N., İmamoğlu R., Türkekul İ., Gökçe İ., Özgür A. (2022). "Biosynthesis and characterization of silver nanoparticles from *Tricholoma ustale* and *Agaricus arvensis* extracts and investigation of their antimicrobial, cytotoxic, and apoptotic potentials." *Journal of Drug Delivery Science and Technology* 69, 103178. <https://doi.org/10.1016/j.jddst.2022.103178>
- [7] Gökşen Tosun N., Kaplan Ö., İmamoğlu R., Türkekul İ., Gökçe İ., Özgür A. (2022). "Green synthesized silver nanoparticles with mushroom extracts of *Paxina leucomelas* and *Rhizopogon luteolus* induce ROS-Induced intrinsic apoptotic pathway in cancer cells." *Inorganic and Nano-Metal Chemistry* 1-10. [10.1080/24701556.2022.2081200](https://doi.org/10.1080/24701556.2022.2081200)
- [8] Kaplan Ö., Gökşen Tosun N., Özgür A., Erden Tayhan S., Bilgin S., Türkekul İ., Gökçe İ. (2021). "Microwave-assisted green synthesis of silver nanoparticles using crude extracts of *Boletus edulis* and *Coriolus versicolor*: Characterization, anticancer, antimicrobial and wound healing activities." *Journal of Drug Delivery Science and Technology* 64, 102641. <https://doi.org/10.1016/j.jddst.2021.102641>
- [9] Rudrappa M., Kumar R.S., Nagaraja S.K., Hiremath H., Gunagambhire P.V., Almansour A.I., Perumal K., Nayaka S. (2023). "Myco-Nanofabrication of Silver Nanoparticles by *Penicillium brasilianum* NP5 and Their Antimicrobial, Photoprotective and Anticancer Effect on MDA-MB-231 Breast Cancer Cell Line." *Antibiotics* 12, 567
- [10] Mikhailova E.O. (2020). "Silver Nanoparticles: Mechanism of Action and Probable Bio-Application." *J Funct Biomater* 11. [10.3390/jfb11040084](https://doi.org/10.3390/jfb11040084)
- [11] Tagde P., Kulkarni G.T., Mishra D.K., Kesharwani P. (2020). "Recent advances in folic acid engineered nanocarriers for treatment of breast cancer." *Journal of Drug Delivery Science and Technology* 56, 101613. <https://doi.org/10.1016/j.jddst.2020.101613>

- [12] Moffatt B.A., Ashihara H. (2002). "Purine and pyrimidine nucleotide synthesis and metabolism." *Arabidopsis Book* 1, e0018. 10.1199/tab.0018
- [13] Zwicke G.L., Mansoori G.A., Jeffery C.J. (2012). "Utilizing the folate receptor for active targeting of cancer nanotherapeutics." *Nano Rev* 3. 10.3402/nano.v3i0.18496
- [14] Martín-Sabroso C., Torres-Suárez A.I., Alonso-González M., Fernández-Carballido A., Fraguas-Sánchez A.I. (2021). "Active Targeted Nanoformulations via Folate Receptors: State of the Art and Future Perspectives." *Pharmaceutics* 14. 10.3390/pharmaceutics14010014
- [15] Luong D., Kesharwani P., Alsaab H.O., Sau S., Padhye S., Sarkar F.H., Iyer A.K. (2017). "Folic acid conjugated polymeric micelles loaded with a curcumin difluorinated analog for targeting cervical and ovarian cancers." *Colloids and Surfaces B: Biointerfaces* 157, 490-502. <https://doi.org/10.1016/j.colsurfb.2017.06.025>
- [16] Sabzichi M., Mohammadian J., Khosroushahi A.Y., Bazzaz R., Hamishehkar H. (2016). "Folate-Targeted Nanostructured Lipid Carriers (NLCs) Enhance (Letrozol) Efficacy in MCF-7 Breast Cancer Cells." *Asian Pacific Journal of Cancer Prevention* 17, 5185-5188. 10.22034/APJCP.2016.17.12.5185
- [17] Xu L., Yang H., Folate-Decorated Polyamidoamine Dendrimer Nanoparticles for Head and Neck Cancer Gene Therapy, in: L. Dinesh Kumar (Ed.) *RNA Interference and Cancer Therapy: Methods and Protocols*, Springer New York, New York, NY, 2019, pp. 393-408.
- [18] Ghaznavi H., Hosseini-Nami S., Kamrava S.K., Irajirad R., Maleki S., Shakeri-Zadeh A., Montazerabadi A. (2018). "Folic acid conjugated PEG coated gold-iron oxide core-shell nanocomplex as a potential agent for targeted photothermal therapy of cancer." *Artificial Cells, Nanomedicine and Biotechnology* 46, 1594-1604. 10.1080/21691401.2017.1384384
- [19] Comşa Ş., Cimpean A.M., Raica M. (2015). "The story of MCF-7 breast cancer cell line: 40 years of experience in research." *Anticancer research* 35, 3147-3154
- [20] Marshalek J.P., Sheeran P.S., Ingram P., Dayton P.A., Witte R.S., Matsunaga T.O. (2016). "Intracellular delivery and ultrasonic activation of folate receptor-targeted phase-change contrast agents in breast cancer cells in vitro." *J Control Release* 243, 69-77. 10.1016/j.jconrel.2016.09.010
- [21] Gökşen Tosun N., Kaplan Ö. (2021). "Optimization of the green synthesis of silver nanoparticle with Box-Behnken design: Using Aloe vera plant extract as a reduction agent." *Sakarya University Journal of Science* 25, 774-787
- [22] Lalegani Z., Seyyed Ebrahimi S.A. (2020). "Optimization of synthesis for shape and size controlled silver nanoparticles using response surface methodology." *Colloids and Surfaces A: Physicochemical and Engineering Aspects* 595, 124647. <https://doi.org/10.1016/j.colsurfa.2020.124647>
- [23] Gökşen Tosun N., Kaplan Ö., Imamoğlu R., Türkekul İ., Gökçe İ., Özgür A. "Green synthesized silver nanoparticles with mushroom extracts of *Paxina leucomelas* and *Rhizopogon luteolus* induce ROS-Induced intrinsic apoptotic pathway in cancer cells." *Inorganic and Nano-Metal Chemistry* 1-10. 10.1080/24701556.2022.2081200
- [24] Subba Rao Y., Kotakadi V.S., Prasad T.N.V.K.V., Reddy A.V., Sai Gopal D.V.R. (2013). "Green synthesis and spectral characterization of silver nanoparticles from Lakshmi tulasi (*Ocimum sanctum*) leaf extract."

- Spectrochimica Acta Part A: Molecular and Biomolecular Spectroscopy 103, 156-159.
<https://doi.org/10.1016/j.saa.2012.11.028>
- [25] Chowdhuri A.R., Tripathy S., Haldar C., Chandra S., Das B., Roy S., Sahu S.K. (2015). "Theoretical and experimental study of folic acid conjugated silver nanoparticles through electrostatic interaction for enhance antibacterial activity." RSC Advances 5, 21515-21524. 10.1039/C4RA16785F
- [26] Xu L., Wang Y.Y., Huang J., Chen C.Y., Wang Z.X., Xie H. (2020). "Silver nanoparticles: Synthesis, medical applications and biosafety." Theranostics 10, 8996-9031. 10.7150/thno.45413
- [27] Bandyopadhyay A., Roy B., Shaw P., Mondal P., Mondal M.K., Chowdhury P., Bhattacharya S., Chattopadhyay A. (2020). "Cytotoxic effect of green synthesized silver nanoparticles in MCF7 and MDA-MB-231 human breast cancer cells in vitro." The Nucleus 63, 191-202. 10.1007/s13237-019-00305-z
- [28] El-Hammadi M.M., Delgado Á.V., Melguizo C., Prados J.C., Arias J.L. (2017). "Folic acid-decorated and PEGylated PLGA nanoparticles for improving the antitumour activity of 5-fluorouracil." International Journal of Pharmaceutics 516, 61-70. <https://doi.org/10.1016/j.ijpharm.2016.11.012>
- [29] Erdoğan N., Esendağlı G., Nielsen T.T., Şen M., Öner L., Bilensoy E. (2016). "Design and optimization of novel paclitaxel-loaded folate-conjugated amphiphilic cyclodextrin nanoparticles." International Journal of Pharmaceutics 509, 375-390. <https://doi.org/10.1016/j.ijpharm.2016.05.040>
- [30] Karuppaiah A., Rajan R., Hariharan S., Balasubramaniam D.K., Gregory M., Sankar V. (2020). "Synthesis and Characterization of Folic Acid Conjugated Gemcitabine Tethered Silver Nanoparticles (FA-GEM-AgNPs) for Targeted Delivery." Curr Pharm Des 26, 3141-3146. 10.2174/1381612826666200316143239
- [31] Kesharwani P., Banerjee S., Gupta U., Mohd Amin M.C.I., Padhye S., Sarkar F.H., Iyer A.K. (2015). "PAMAM dendrimers as promising nanocarriers for RNAi therapeutics." Materials Today 18, 565-572. <https://doi.org/10.1016/j.mattod.2015.06.003>
- [32] Banu H., Sethi D.K., Edgar A., Sheriff A., Rayees N., Renuka N., Faheem S.M., Premkumar K., Vasanthakumar G. (2015). "Doxorubicin loaded polymeric gold nanoparticles targeted to human folate receptor upon laser photothermal therapy potentiates chemotherapy in breast cancer cell lines." Journal of Photochemistry and Photobiology B: Biology 149, 116-128. <https://doi.org/10.1016/j.jphotobiol.2015.05.008>
- [33] Kumar P., Tambe P., Paknikar K.M., Gajbhiye V. (2017). "Folate/N-acetyl glucosamine conjugated mesoporous silica nanoparticles for targeting breast cancer cells: A comparative study." Colloids and Surfaces B: Biointerfaces 156, 203-212. <https://doi.org/10.1016/j.colsurfb.2017.05.032>
- [34] Kesharwani P., Choudhury H., Meher J.G., Pandey M., Gorain B. (2019). "Dendrimer-entrapped gold nanoparticles as promising nanocarriers for anticancer therapeutics and imaging." Progress in Materials Science 103, 484-508. <https://doi.org/10.1016/j.pmatsci.2019.03.003>
- [35] Assaraf Y.G., Leamon C.P., Reddy J.A. (2014). "The folate receptor as a rational therapeutic target for personalized cancer treatment." Drug Resistance Updates 17, 89-95. <https://doi.org/10.1016/j.drug.2014.10.002>

- [36] Ramzy L., Nasr M., Metwally A.A., Awad G.A.S. (2017). "Cancer nanotheranostics: A review of the role of conjugated ligands for overexpressed receptors." *European Journal of Pharmaceutical Sciences* 104, 273-292. <https://doi.org/10.1016/j.ejps.2017.04.005>
- [37] Xu L., Bai Q., Zhang X., Yang H. (2017). "Folate-mediated chemotherapy and diagnostics: An updated review and outlook." *Journal of Controlled Release* 252, 73-82. <https://doi.org/10.1016/j.jconrel.2017.02.023>
- [38] Darvish S., Saeed Kahrizi M., Özbolat G., Khaleghi F., Mortezaia Z., Sakhaei D. (2022). "Silver nanoparticles: Biosynthesis and cytotoxic performance against breast cancer MCF-7 and MDA-MB-231 cell lines." *Nanomedicine Research Journal* 7, 83-92